NASA TECHNICAL MEMORANDUM 104049

FRACTURE MECHANICS ANALYSIS FOR VARIOUS FIBER/MATRIX INTERFACE LOADINGS

R. A. Naik and J. H. Crews, Jr.

February 1991

National Aeronautics and
Space Administration

Langley Research Center
Hampton, Virginia 23665

ABSTRACT

Fiber/matrix (F/M) cracking was analyzed to provide better understanding and guidance in developing F/M interface fracture toughness tests. Two configurations, corresponding to F/M cracking at a broken fiber and at the free edge, were investigated. The effects of mechanical loading, thermal cooldown and friction were investigated. Each configuration was analyzed for two loadings: longitudinal and normal to the fiber. A nonlinear finite element analysis was performed to model friction and slip at the F/M interface. A new procedure for fitting a square-root singularity to calculated stresses was developed to determine stress intensity factors (K_I and K_{II}) for a bimaterial interface crack. For the case of F/M cracking at a broken fiber with longitudinal loading, crack tip conditions were strongly influenced by interface friction. As a result, a F/M interface toughness test based on this case was not recommended because nonlinear data analysis methods would be required. For the free edge crack configuration, both mechanical and thermal loading caused crack opening, thereby avoiding frictional effects. A F/M interface toughness test based on this configuration would provide data for K_I/K_{II} ratios of about 0.7 and 1.6 for fiber and radial normal loading, respectively. However, thermal effects must be accounted for in the data analysis.

KEYWORDS: Composites, interface, stress intensity factors, fracture, finite element analysis.

INTRODUCTION

The fracture of advanced composite materials can involve three types of local failures: fiber fracture, matrix cracking, and fiber-matrix (F/M) debonding. While the properties of the fiber and the matrix are important governing factors, the fracture toughness of the F/M interface is critical to the failure process and overall composite toughness. A characterization of F/M interface toughness is, therefore, essential in the development of tougher composites.

The analysis of F/M cracking is complicated by the fact that it involves crack growth at the interface between two different materials. Differences in elastic properties across the interface can lead to mixed-mode fracture conditions at the crack tip even when the geometry and loading are symmetric with respect to the crack [1]. The analysis is further complicated by the presence of thermal residual stresses and friction at the F/M interface. Numerical analyses [2] have been used in the past to calculate stress intensity factors (K_1 and K_2) for cracks at a bimaterial interface. However, the definitions for K_1 and K_2 [1] did not represent opening and shear stresses, respectively, and, thus, the results did not provide the usual physical interpretation associated with the classical K_I and K_{II}.

To characterize F/M interface toughness for a particular F/M combination, it might be necessary to perform tests over a wide range of mixed-mode ratios. Although there are a few tests to measure F/M interface strength [3], there are currently no tests available to determine F/M toughness. The purpose of this study was to investigate two different configurations (Fig. 1), from a fracture mechanics standpoint, to provide some of the understanding and guidance needed to develop a F/M interface toughness test. The two configurations in Fig. 1 approximate a single fiber in a matrix and correspond to F/M cracking at a broken fiber and at the free edge. Each configuration was analyzed for two loadings: (i) longitudinal and (ii) normal to the fiber. Note

that the two loadings were not applied simultaneously and the analysis involved only uniaxial loading cases.

A finite element analysis was used to analyze F/M cracking for the two configurations. The effects of mechanical (longitudinal and normal) loading, thermal cooldown, and F/M interface friction were investigated. A new finite element based procedure was developed for calculating K_I and K_{II} for a bimaterial crack. Results are presented and discussed in terms of total strain energy release rates G_T, K_I, and K_{II} for the different cases considered.

ANALYSIS

Both the configurations analyzed in the present study were axisymmetric about the fiber direction. F/M cracking near a broken fiber end (Fig. 1(a)) was analyzed for two cases: loading in the fiber direction and axisymmetric loading normal to the fiber. Due to symmetry about the fiber break, only one half of the model needed to be analyzed. F/M cracking at the free edge (Fig. 1(b)) was analyzed as two additional cases: a fiber pullout load and axisymmetric tension normal to the fiber. Both configurations were analyzed for thermal effects after cooldown. The effects of friction at the F/M interface were also analyzed. All these cases were analyzed by applying different boundary conditions to the same axisymmetric model. The MSC/NASTRAN finite element code [4] was used for the analysis. Transversely isotropic and isotropic properties were used for the graphite (AS4) fiber and the epoxy (3501-6) matrix [5], respectively (Table I).

Axisymmetric Model: A 2-degree wedge shaped model was used (Fig. 2(a)). Since the 2-D axisymmetric elements in MSC/NASTRAN are limited to linear analysis, a 3-D model was used. The fiber and the matrix were modelled discretely and all dimensions were selected relative to the fiber diameter d. The model length and width were both 10d. To compare the candidate

configurations, a single crack length ($a = d$) was used for all cases. The origin of the cylindrical coordinate system R-θ-Z was located at the top left corner of the model with the Z-axis in the fiber direction. The symbols u, v, and w represented displacements in the R, θ, and Z directions, respectively.

As shown in Table II, to simulate the different cases, different boundary conditions were imposed on the model. Axisymmetry was imposed for all cases by requiring $v=0$ on the $\theta=0$ and 2^{o} planes and also requiring $u=0$ along the fiber axis EE. For all cases, the surfaces AA and CC were constrained to remain planar and the surface BB was constrained to remain cylindrical during deformation. These boundary conditions were implemented in the finite element analysis by multi-point constraints [4] at surface nodes. For the broken fiber case with thermal cooldown, $w = 0$ was imposed on the fiber surface DD because the fiber ends will transmit compression. For purposes of superposing mechanical and thermal loading, two sets of boundary conditions were required for longitudinal loading: one for fiber ends remaining in contact and one for loading beyond that required to separate the fiber ends. Similarly, two sets of boundary conditions were required for normal loading, as shown in Table II.

Finite Element Mesh: A section (along $\theta = 0$) of the finite element mesh is shown in Fig. 2(b). A local coordinate system x-y has its origin at the crack tip and the x-axis in the crack growth direction. Eight noded isoparametric hexahedron elements were used everywhere except along the fiber axis where a layer of six noded isoparametric pentahedron elements was used. In the vicinity of the crack tip, a very fine mesh was used (Fig. 2(c)) because of the singularity there. The smallest elements with length Δ were next to the crack tip with element lengths doubling in the x and y directions. To prevent the crack faces from interpenetrating, special "gap elements" were used between the nodes across the crack face (Fig. 2(c)). These gap elements should, ideally, have very high compressive and shear stiffnesses, however, to prevent numerical

problems, they were chosen to be the same as the neighboring fiber elements. The tensile stiffness of the gap elements was almost negligible [4]. The shear response was linear up to the frictional limit. An incremental nonlinear analysis was performed to model slip beyond the frictional limit of the gap elements (i.e. along the crack faces) for a prescribed coefficient of friction.

The adequacy of the mesh refinement was evaluated by a convergence study of a large homogeneous plate (crack length/width = 0.1, model length/width = 3.0) with a center crack and Mode I loading. The computed stresses and stress intensity factor K (calculated by the method described in the next section) were compared with closed-form solutions. For a mesh refinement of $\Delta/a = 5\times10^{-6}$, the calculated K was within 2.5% of the handbook value [6]. The distribution of opening stress (σ_{yy}) versus distance ahead of the crack tip was plotted on a log-log plot to see how its slope compared with -0.5. In the region $1\times10^{-5} \leq (x/a) \leq 2\times10^{-2}$, its slope was -0.495. The mesh refinement of $\Delta/a = 5\times10^{-6}$ was, therefore, used for the present analysis. However, since the present study involves cracks at bi-material interfaces, a second comparison was made. The computed stresses for a interface crack in a large aluminum/epoxy plate (crack length/width = 0.1, length of each material/width = 1.5), with Mode I loading, were compared with a closed-form solution [1]. As shown in Fig. 3(a), the comparison is quite satisfactory. Because the stiffness of aluminum is more than 20 times that of epoxy, the aluminum/epoxy case was comparable to the graphite/epoxy cases analyzed in this paper.

Calculation of G_T and K_I and K_{II}: The total strain energy release rate G_T was calculated using the virtual crack closure technique [7]. For a crack at a bimaterial interface, while the G_T shows convergence with increasing mesh refinement, the Mode I and Mode II components of the strain energy release rate do not converge [8]. Thus, it is necessary to use some other means to

characterize the mixed mode conditions near the interface crack tip. An alternative is to use stress intensity factors. However, the stress intensity factors (K_1 and K_2) defined by Rice [1] and Suo and Hutchinson [9] for a bimaterial crack also have certain limitations. For example, in contrast to the homogeneous case, K_1 and K_2 are not strictly associated with opening and shear stresses, respectively [10]. Moreover, K_1 and K_2 are functions of an arbitrary length parameter making them functions of the system of units in which they are defined [10].

These problems are a result of the peculiar singularity at a bimaterial crack which is of the order $r^{-(1/2) + i\epsilon}$ where r is the radial distance from the crack tip, ϵ is a bimaterial constant and $i = \sqrt{-1}$ [1]. Fortunately, the region of influence of the $r^{i\epsilon}$ term has been shown to be of the order of 10^{-6} to 10^{-8} times the crack length [11]. Thus, for practical materials the region of $r^{i\epsilon}$ influence is probably small compared to the plastic zone at an advancing crack tip. Therefore, crack tip plasticity probably prevents the $r^{i\epsilon}$ influence from developing or at least limits its significance. However, the $r^{(-1/2)}$ singularity and the conventional stress intensity factors should still characterize the stress field surrounding the crack tip, provided the plastic zone is small compared to the crack length. Arguments for approximating the bimaterial crack-tip stresses by a $r^{-(1/2)}$ singularity have also been advanced in references 9 and 11. For these reasons, both the normal and shear stresses near the crack-tip were assumed to have the form [12,13]

$$\sigma = \frac{K}{\sqrt{(2\pi r)}} + A \qquad (1)$$

where K is a stress intensity factor and A is a constant.

The stress intensity factors K_I and K_{II} were determined from a least squares fit of Eq. (1) to the calculated normal and shear stresses,

respectively. The curve-fitting was performed in the region $1x10^{-5} \leq (x/a) \leq 2x10^{-2}$ (Fig. 3(b)) as this was found to be adequate for the homogeneous case. The curve-fit in this particular case had a coefficient of variation of 0.9999 for the normal stress and 0.995 for the shear stress. For all other cases, coefficients of variation were between 0.9996 and 0.9965 except for the crack at the broken fiber case (with longitudinal loading) which had a value of 0.986. Thus, this simple finite element based procedure was considered to be quite satisfactory for computing meaningful values of K_I and K_{II} for a crack at a bimaterial interface. For cases in which the crack faces closed, the gap elements kept the crack faces from crossing and only a K_{II} was calculated.

For the thermal cases, it was arbitrarily assumed that residual stresses would build up during the last 100°C of the curing cycle and, thus, G_T , K_I and K_{II} were calculated for a 100°C decrease in temperature. Since the present analysis would not be valid beyond the yield point of the matrix, G_T, K_I and K_{II} were calculated for an applied matrix stress of 82.7 MPa which is the yield stress of the epoxy matrix [14].

RESULTS AND DISCUSSION

Results for all the cases are presented in terms of G_T, K_I, K_{II} and K_I/K_{II} in Table III. The results for the F/M crack at the broken fiber are discussed first, followed by results for the F/M crack at the free edge.

F/M Crack at a Broken Fiber: Thermal cooldown, in this case, causes the two ends of the broken fiber to contact and also introduces compressive radial stresses along the crack faces. For the cooldown of 100° C, an average compressive radial stress of 8.5 MPa was computed. Table III shows that G_T, K_I and K_{II} are all zero for this case, as expected, since there are no opening and shear stresses along the crack faces.

The longitudinal loading case also resulted in crack closure. Analyses were conducted for two different coefficients of friction: μ = 0 and 0.1. For both μ=0 and μ=0.1, there was slip along the entire crack length. For the linear μ=0 case, K_I was zero, as expected, and K_{II} was 549.3 MPa$\sqrt{m}$ and G_T was 28.33 MJ, as shown in Table III. For the nonlinear μ=0.1 case, K_I was again zero but K_{II} was reduced by 40% to 331.3 MPa$\sqrt{m}$, and G_T was reduced by a factor of 12, compared to the μ=0 case. If thermal cooldown had been combined with this nonlinear case, even higher frictional stresses would have developed and K_{II} and G_T would have been smaller yet. In general, frictional slip requires nonlinear analysis methods. Therefore, this case is not recommended as a candidate F/M interface toughness test.

For the frictionless case, longitudinal loading can be superposed on the thermal cooldown effects. For superposed longitudinal loading less than 21.6 MPa the fiber ends remained in contact and the K_I, K_{II} and G_T were zero. For superposed loading equal to matrix yield (82.7 MPa), K_I continued to be zero, but Table III shows that K_{II} reduced by 26% and Fig. 4(a) shows G_T reduced by 45%. Therefore, if a frictionless interface crack can be achieved, the longitudinal case could provide an interface toughness test for pure mode II conditions, but thermal effects need to be accounted for.

Although an axisymmetric normal load is difficult to achieve in practice, it does represent a baseline case for a F/M crack under mode I loading. This mode I loading, however, produces a mixed-mode condition at the crack tip. Fig. 4(b) shows a K_I/K_{II} ratio of 1.76 for this case. Since normal loading causes crack opening, there are no frictional effects and this linear case can be superposed on the thermal case. Thermal residual stresses delayed crack opening until the applied stress was 7.2 MPa. Results in Fig. 4(b), for an applied stress of 82.7 MPa, show that there is no change in the K_I/K_{II} ratio when mechanical and thermal loadings are combined. However, this superposition reduced G_T by 17% (see Table III and Fig. 4(a)). In general, this normal

loading case would be a candidate test case, provided the cooldown stresses are accounted for and the radial loading can be applied by simple means. However, because of its low G_T value, matrix cracking could develop before F/M cracking.

F/M Crack at the Free Surface: Unlike the broken fiber case, thermal cooldown caused crack opening for this case and a non-zero G_T. Fiber pullout loading also led to crack opening. Thus, there were no frictional effects in this case. Fig. 4(a) shows that G_T is much higher than the broken fiber case. However, Fig. 4(b) shows that the K_I/K_{II} ratio is lower, 0.69 compared to 1.76. Superposition of the thermal and fiber loading cases (Table III) led to higher values for K_I and K_{II} and a small decrease in the K_I/K_{II} ratio (Fig. 4(b)). Thermal effects produced a 12% increase in G_T. Note that when mechanical and thermal loadings are superposed, the resulting G_T is not simply the sum of the G_T values for the two loadings. The calculation of G_T involves the product of forces and displacements; therefore, cross products develop when two cases are added. It should also be noted that, since the fiber loading case has a very high G_T value, F/M cracking could become critical at very small loads. The fiber pullout loading appears to be a viable approach for F/M interface toughness testing.

Fig. 4(b) shows that axisymmetric normal load had a larger proportion of mode I than the corresponding broken fiber case. Also, the G_T value, for this case, was about four times that for the broken fiber case but still fairly low. Since there was crack opening in this case, there were no frictional effects. The superposition of thermal and mechanical stresses led to a 43% increase in the G_T and a 30% decrease in the K_I/K_{II} ratio. For such superposition, the K_I/K_{II} ratio is a function of the applied load level. Without mechanical loading, the K_I/K_{II} ratio was 0.45 due to thermal cooldown effects alone. This ratio increased to 1.6 when the applied stress in the matrix equalled the matrix yield stress (82.7 MPa). This case would be suitable for toughness testing,

provided the effects of thermal cooldown are accounted for. Note that thermal cooldown effects will be reduced due to counteracting moisture effects.

SUMMARY

Fiber/matrix (F/M) cracks were analyzed for two different configurations representing F/M cracking at a broken fiber and at a free edge. The effects of mechanical loading, thermal cooldown, and interface friction were investigated. A nonlinear finite element analysis was used to model friction and slip at the F/M interface. A new procedure for fitting a square-root singularity to the calculated stresses was developed. This provided classical K_I and K_{II} values for a bimaterial interface crack.

For the case of F/M cracking at a broken fiber (with longitudinal loading), friction (μ=0.1) along the debond length, led to a 40% decrease in K_{II} and a 12-fold decrease in G_T. Thermal residual stresses were compressive and, therefore, would produce additional frictional effects. A F/M interface toughness specimen based on this configuration would be strongly influenced by frictional effects.

For the free edge crack configuration, thermal cooldown caused crack opening and led to a non-zero G_T. Fiber loading produced a high G_T value suggesting F/M cracking as the critical failure mode. Axisymmetric normal loading produced a 2.25 K_I/K_{II} ratio which decreased by 30% due to thermal cooldown effects. Both mechanical loading and thermal cooldown caused crack opening, precluding frictional effects. A F/M interface toughness test based on this configuration would provide data for K_I/K_{II} ratios of about 0.7 (pullout load) and 1.6 (normal load). However, thermal cooldown effects need to be accounted for.

REFERENCES

1. Rice, J. R.; "Elastic Fracture Mechanics Concepts for Interfacial Cracks," J. App. Mech., Vol. 55, March 1988, pp. 98-103.
2. Smelser, R. E.; "Evaluation of Stress Intensity Factors for Bimaterial Bodies Using Numerical Crack Flank Displacement Data," Int. J. Frac., Vol. 15, No. 2, 1979, pp. 135-143.
3. Narkis, M., et. al.; "Review of Methods for Characterization of Interfacial Fiber-Matrix Interactions," Poly. Comp., Vol. 9, No. 4, Aug. 1988, pp. 245-251.
4. MSC/NASTRAN User's Manual, Vols. 1 and 2, Nov. 1989. The MacNeal-Schwendler Corporation, Los Angeles, California.
5. Adams, D. F. and Schaffer, B. G.; "Analytical/Experimental Correlations of Stiffness Properties of Unidirectional Composites," Comp. Tech. Rev., Vol. 4, No. 2, 1982, pp. 45-48.
6. Tada, H., Paris, P. C. and Irwin, G.; "The Stress Analysis of Crack Handbook," 2nd Edition, Paris Production Incorporated (and Del Research Corporation), St. Louis, Missouri, 1985.
7. Rybicki, E. F. and Kanninen, M. F.; "A Finite Element Calculation of Stress Intensity Factors by Modified Crack Closure Integral," Eng. Frac. Mech., Vol 9., 1977, pp. 931-938.
8. Raju, I. S. et. al.; "Convergence of Strain Energy Release Rate Components for Edge-Delaminated Composite Laminates," Eng. Frac. Mech., Vol. 30, No. 3, 1988, pp. 383-396.
9. Suo, Z. and Hutchinson, J. W.; "Sandwich Test Specimen for Measuring Interface Crack Toughness," Mat. Sc. and Eng., A107, 1989, pp. 135-143.
10. Sawyer, S. G. and Anderson, R. B.; "Collocated Interfacial Stress Intensity Factors for Finite Bi-Material Plates," Eng. Frac. Mech., Vol. 4, 1972, pp. 605-616.

11. Wang, S. S. and Choi, I.; "The Interface Crack Between Dissimilar Anisotropic Composite Materials," J. App. Mech., Mar. 1983, Vol. 50, pp. 169-178.

12. Raju, I. S.; "Calculation of Strain-Energy Release Rates with Higher Order and Singular Finite Elements," Eng. Frac. Mech., Vol. 28, No. 3, pp. 251-274, 1987.

13. Irwin, G. R.; "Analysis of Stresses and Strains Near the End of a Crack Traversing a Plate," J. Appl. Mech., Vol. 24, 1957, pp. 361-364.

14. Johnston, N. J. and Hergenrother, P. M.; "High Performance Thermoplastics: A Review of Neat Resin and Composite Properties," Proc. 32nd Sampe Sym. and Exhibition, Anaheim, CA, April 1987.

Table I.- Constituent material properties [5].

	E_Z (GPa)	E_R (GPa)	G_{ZR} (GPa)	G_{RR} (GPa)	ν_{ZR}	ν_{RR}	α_Z ($10^{-6}/^{o}C$)	α_R ($10^{-6}/^{o}C$)
Fiber (AS4)	220	13.8	34	5.5	0.20	0.25	-0.36	18.0
Matrix (3501-6)	4.3	4.3	1.6	1.6	0.34	0.34	40.00	40.0

Table II.- Boundary conditions used for axisymmetric model.

Case	Crack faces	Boundary Conditions Along: AA (bottom)	BB (cylinder)	CC (matrix)	DD (fiber)
F/M crack at broken fiber					
(i) Thermal cooldown	Gap*	w=const.	u=const.	w=0	w=0
(ii) Long. loading (before fiber end separation)	Gap	w=0.05	u=const.	w=0	w=0
(iii) Long. loading (after fiber end separation)	Gap	w=0.05	u=const.	w=0	free
(iii) Normal loading (before crack opening)	MPC**	w=const.	u=0.05	w=0	w=0
(iv) Normal loading (after crack opening)	free	w=const.	u=0.05	w=0	w=0
F/M crack on free edge					
(i) Thermal cooldown	free	w=0	u=const.	free	free
(ii) Fiber loading	free	w=0	u=const.	free	w=-0.05
(iii) Normal loading	free	w=0	u=0.05	free	free

*Gap elements prevented interpenetration and modeled friction along crack.

**MPC - multi-point constraints forced u-displacements of adjacent nodes along the crack to be equal.

Table III.- Strain energy release rates and stress intensity factors.

Case	G_T(MJ/m^2)	K_I(MPa$\sqrt{m}$)	K_{II}(MPa$\sqrt{m}$)	K_I/K_{II}
F/M crack at broken fiber				
(i) Thermal cooldown	0.00	0.00	0.0	0.00
(ii) Longitudinal loading (μ=0)	28.33	0.00	549.3	0.00
(iii) Longitudinal loading (μ=0.1)	2.22	0.00	331.3	0.00
(iv) Thermal + longitudinal (μ=0)	15.45	0.00	405.8	0.00
(v) Normal loading	8.66	317.5	180.7	1.76
(vi) Thermal + normal loading	7.22	289.9	165.0	1.76
F/M crack on free edge				
(i) Thermal cooldown	4.06	78.9	176.5	0.45
(ii) Fiber pullout loading	341.40	1419.0	2067.0	0.69
(iii) Thermal + fiber loading	383.50	1497.0	2243.1	0.67
(iv) Normal loading	34.03	697.8	310.1	2.25
(v) Thermal + normal loading	48.84	776.7	486.6	1.60

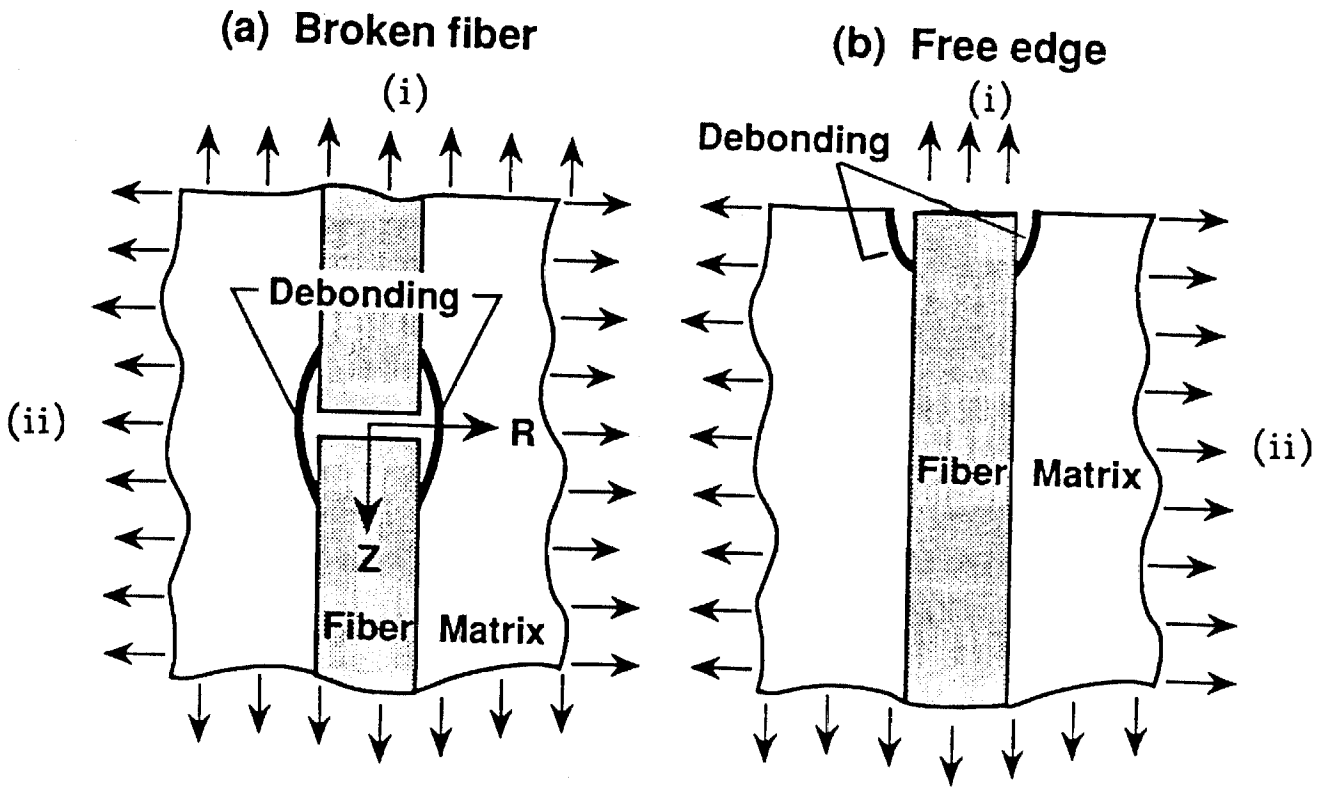

Fig. 1.- Fiber/matrix cracking configurations.

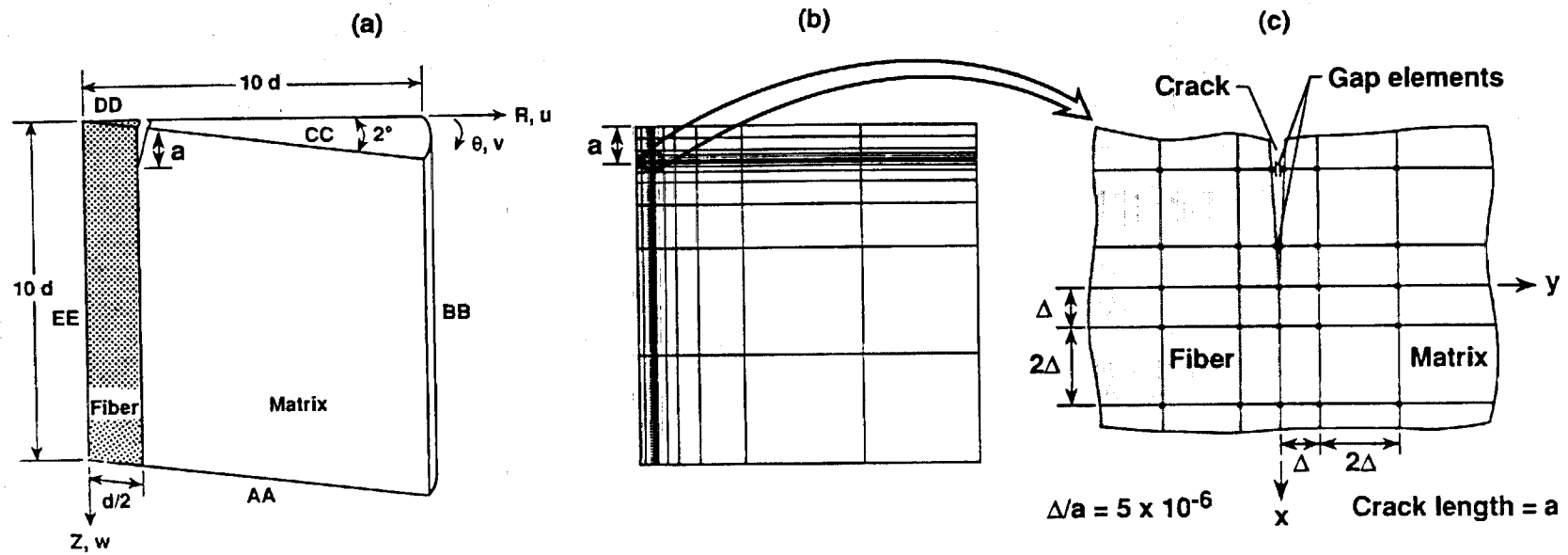

Fig. 2.- Axisymmetric model and finite element mesh.

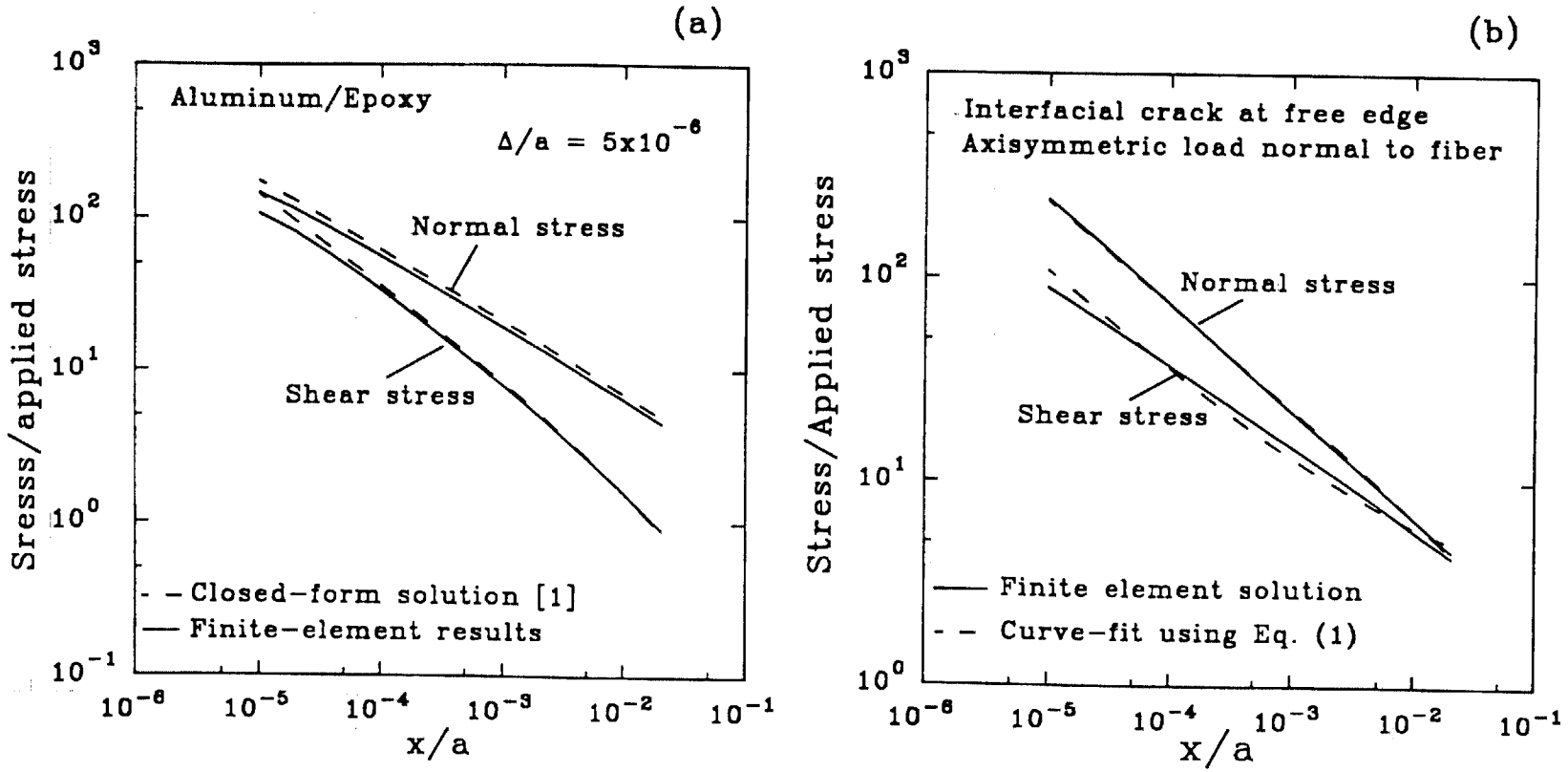

Fig. 3.- Verification of finite element results and curve-fitting procedure.

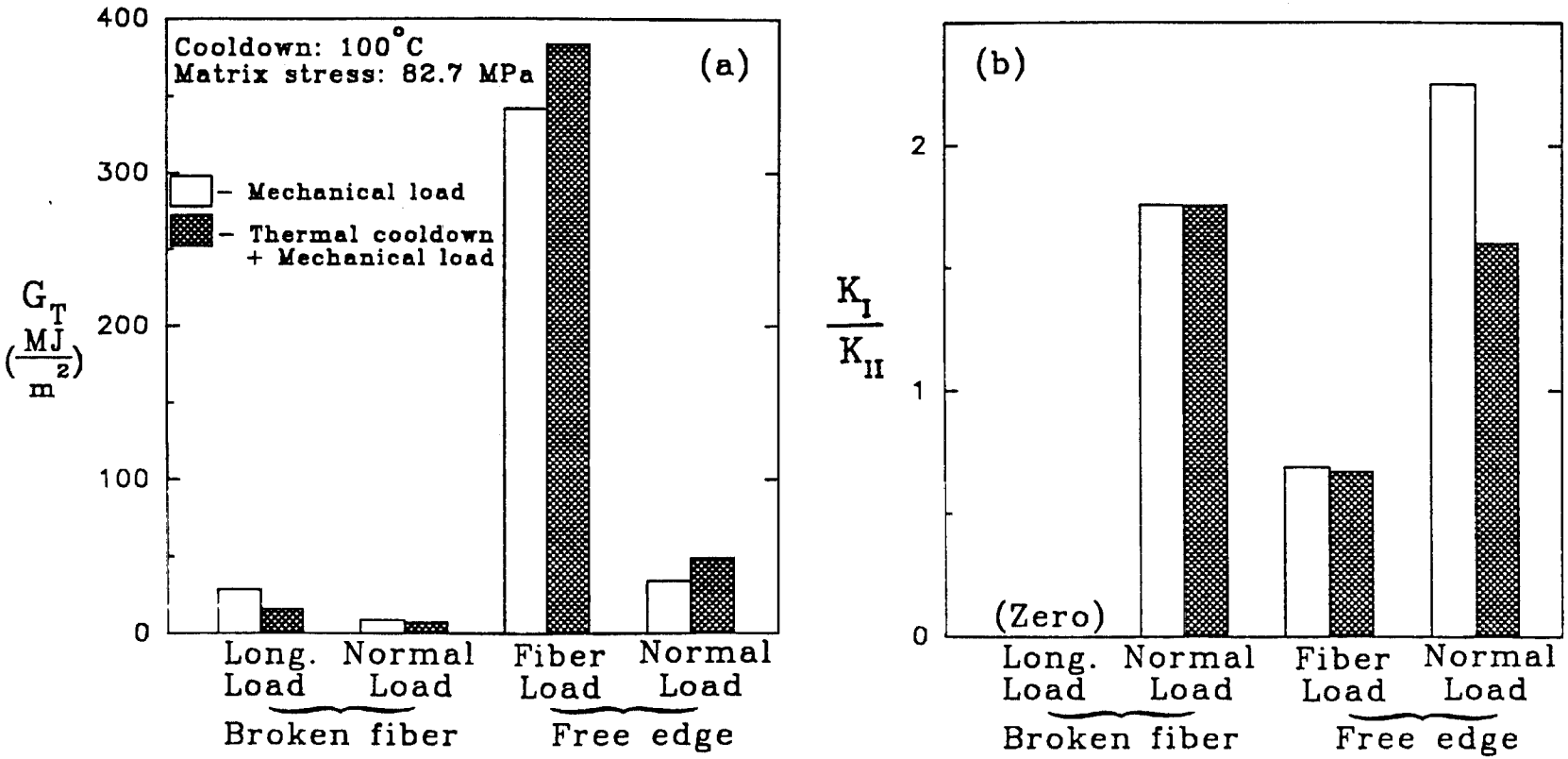

Fig. 4.- Comparison of G_T and K_I/K_{II} values for the different cases.

NASA

Report Documentation Page

1. Report No.	2. Government Accession No.	3. Recipient's Catalog No.
NASA TM-104049		

4. Title and Subtitle	5. Report Date
Fracture Mechanics Analysis for Various Fiber/Matrix Interface Loadings	February 1991
	6. Performing Organization Code

7. Author(s)	8. Performing Organization Report No.
R. A. Naik* and J. H. Crews, Jr.	
	10. Work Unit No. 505-63-50-04

9. Performing Organization Name and Address	11. Contract or Grant No.
NASA Langley Research Center Hampton, VA 23665-5225	
	13. Type of Report and Period Covered: Technical Memorandum
12. Sponsoring Agency Name and Address National Aeronautics and Space Administration Washington, DC 20546	14. Sponsoring Agency Code

15. Supplementary Notes

*R. A. Naik, Analytical Services and Materials, Inc., Hampton, VA

16. Abstract

Fiber/matrix (F/M) cracking was analyzed to provide better understanding and guidance in developing F/M interface fracture toughness tests. Two configurations, corresponding to F/M cracking at a broken fiber and at the free edge, were investigated. The effects of mechanical loading, thermal cooldown and friction were investigated. Each configuration was analyzed for two loadings: longitudinal and normal to the fiber. A nonlinear finite element analysis was performed to model friction and slip at the F/M interface. A new procedure for fitting a square-root singularity to calculated stresses was developed to determine stress intensity factors (K_I and K_{II}) for a bimaterial interface crack. For the case of F/M cracking at a broken fiber with longitudinal loading, crack tip conditions were strongly influenced by interface toughness test based on this case was not recommended because nonlinear data analysis methods would be required. For the free edge crack configuration, both mechanical and thermal loading caused crack opening, thereby avoiding frictional effects. A F/M interface toughness test based on this configuration would provide data for K_I/K_{II} ratios of about 0.7 and 1.6 for fiber and radial normal loading, respectively. However, thermal effects must be accounted for in the data analysis.

17. Key Words (Suggested by Author(s))	18. Distribution Statement
Composites Interface Stress intensity factors Fracture Finite element analysis	Unclassified - Unlimited Subject Category - 24

19. Security Classif. (of this report)	20. Security Classif. (of this page)	21. No. of pages	22. Price
Unclassified	Unclassified	20	A03